An IoT Self Organizing Network for 5G Dense Network Interference Alignment

Anil Kumar Yerrapragada*, Brian Kelley†
Department of Electrical and Computer Engineering, University of Texas at San Antonio
San Antonio, Texas 78249
Email: *anilkumar.yerrapragada@utsa.edu, †dr.brian.kelley@gmail.com,

***Abstract*—To achieve 1000X improvements in capacity, 5G communication networks integrate a heterogenous combination of advanced systems to increase data rate. A significant component of the improvement addressed in this paper, network densification, incorporates closely spaced radio access antennas to achieve high information rates. However, 5G multi-user networks must cope with unprecedented levels of interference and are also susceptible to jamming. To realize high 5G channel capacity targets of 1 Gbps, interference management systems are a necessity. We present, a self organizing Internet of Things (IoT) network infrastructure for protecting the future 5G communication system network from self-induced co-channel interference. We introduce protocols for an IoT based interference-alignment approach. Our main contributions are the introduction of an IoT architecture capable of 5G interference alignment and a spatial dimensioning algorithm that accounts for estimation error in the 5G channel state associated with interference cancellation.**

I. Introduction

The evolution of 5G technology ushers in 1,000-fold gains in cellular capacity, connects 50-500 billion devices, and supports a wide range of data rates, latency, reliability, energy consumption, and device cost requirements [1]. A 1,000 fold capacity gain has three primary contributing factors, spectrum enhancement, spectral efficiency, and network densification.

$$CapGain = Spectrum \times SpectEff \times Densification \quad (1)$$

Several key stake holders have expressed their view on the magnitude of these factors. These factors are summarized in Table 1. Zander and Mhnen [2] argue that even though there is plenty of spectrum available, it is mostly on frequency bands above 10 GHz. This makes it less attractive to cellular styles of operations and more localized in nature. MIMO techniques such as network MIMO, massive MIMO (M-MIMO), and millimeter wave MIMO are potential technologies to achieve spectral efficiency gains needed for 5G. Network MIMO includes coordinated multipoint transmission (CoMP) [3] and Distributed Antenna System (DAS) [4] as possible system architectures. One of the challenges of network MIMO is the large signaling overhead that is needed for the base stations or ENodeBs to cooperate. The 24X spectral efficiency gain assumed by NTTDocomo is likely to be very optimistic. In theory, such a high gain could be achieved by using M-MIMO, but many practical restrictions still need to be investigated [5]. Due to scarcity of good spectrum and challenges in achieving high physical layer capacity gains, densification is likely to play a major role in achieving the 1000X capacity gain. Densification and heterogeneous networks are also critical in providing the capacity for indoor users. In fact it is indoors where the mobile Internet traffic is growing the most [2], [6]. Cloud Radio Access Networks (C-RAN) were introduced by

TABLE I
5G Capacity Increase Table

Author	Spectrum	Spectral Efficiency	Densification	Total Capacity Increase
NSN	10X	10X	10X	1000X
Huawei	3X	3.3X	10X	100X
NTT Docomo	2.8X	24X	15X	1000X
Zander & Mähönen	3X	5X	66X	1000X

China mobile [7] as a key element in achieving the 1000X capacity gain in a cost and energy efficient manner. In C-RAN, the radio access network (RAN) functionality is moved to cloud computing infrastructure [8]. Remote radio units (RRU) [9] of different cells are connected to the cloud via a high speed front-haul link, such as a fiber network. Unlike classical cellular systems where a baseband processing unit is deployed in each cell cite, C-RAN has a central processing system in the cloud.

This architectural change has a number of advantages in terms of capital expenditures (CAPEX) and operational expenditures (OPEX) relative to traditional base stations. Due to centralized processing, C-RAN provides flexibility in terms of signal processing complexity and coordination among cells and networks. Furthermore, it enables Internet-of-Things (IoT) devices to be efficiently deployed [10] to cellular infrastructure. We propose the use of an IoT framework to support "network-densification" with low power IoT devices enabling high capacity, especially in hotspots. In this scenario, IoT configured as an Infrastructure-as-as-Service (IaaS) enables high capacity communications. Hence, inter-cell coordination and joint processing, can be deployed as an IoT overlay for C-RAN. This achieves the maximum 5G link capacity gain.

A. IoT Architecture Model for 5G Interference Alignment

Our central goal is to construct an IoT network, on top of a dense 5G network. The purpose of the IoT overlay

is the cancellation of high levels of interference found in dense 5G communication networks. We focus, without a loss of generality, on the downlink. The ENodeB communication transmitters in the Radio Access Network (RAN) communicate in a downlink fashion to all IoT devices concurrently, but in a coordinated way using precoders whose coefficients are multi-user channel dependent. In combination with beamformers at the IoT devices, the IoT devices cancel system-wide interference across the entire IoT device network. The precoders at the ENodeB are combined with beamformers at the IoT devices.

We choose to adopt a Level-6 IoT architecture as defined in [11]. Each of the K IoT devices communicate to each of the K ENodeBs allocating a portion of their signal power to each ENodeB in a macro-diversity communication framework optimized to cancel the high levels of network interference. This Multi-point to Multi-point configuration corresponds to an $K_M \times K_M$ MIMO channel with $K_M = M \times K$, M antennas per ENodeB and M antennas per IoT device. The Multi-point to Multi-point system utilizes M antenna MIMO capable of full-duplex communication between K IoT devices and K ENodeBs.

The IoT devices measure the receiver channels and send digital actuation across a feedback channel to the ENodeB, indicating the receiver channel coefficients. The cloud application host stores multi-user channel information in its cloud database. Cloud analytics include measurement of the interference at the IoT device with and without interference cancellation using precoding and beamforming computation. A host application, the cloud multi-user interference canceler, collects observer data and sensed communication and control services to each of the IoT devices over RESTful APIs. The host Application and the controller that coordinates the interference system is configured as a cloud application capable of centralized control of the multiple IoT device controllers. The multiple independent end nodes sense signal power, measure interference levels, send digital information to the ENodeB precoders, and collect IoT observation data.

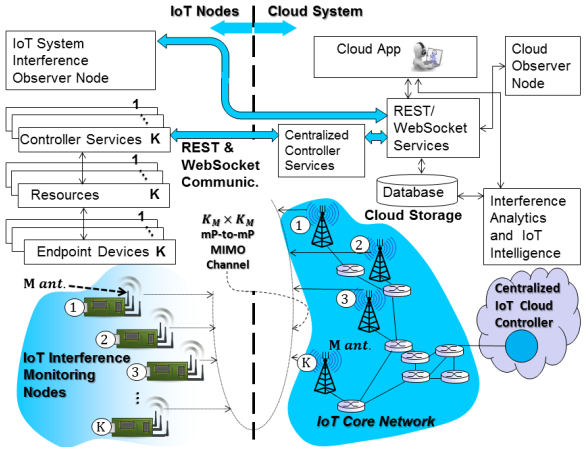

Fig. 1. K Iot architecture for Interference Alignment in Communication Networks

II. Interference Alignment Scheme

Interference alignment mitigates co-channel interference via the application of precoders, applied to transmit signals, and beamformers, applied at the receivers. As a result, the interference can be aligned in such a way that the interference-free space is maximized. The authors in [12] have provided an analysis on interference alignment and degrees of freedom in K user interference channels. In [13], a distributed iterative algorithm for obtaining the precoders and beamformers by making use of the dual relationship between interference alignment on a channel and its reciprocal with communication direction reversed, is presented. A perfect interference alignment algorithm using zero forcing beamformers has been proposed in [14]. It is on this framework, that we base our IoT interference cancellation model.

A. K device Network Model

Let K be the number of ENodeBs and IoT devices. We assume an $M \times M$ MIMO scenario in which M is even and equal to $K(K-1)$. Fig. 1 shows the MIMO network model. Table II shows the nomenclature of the variables used in this paper.

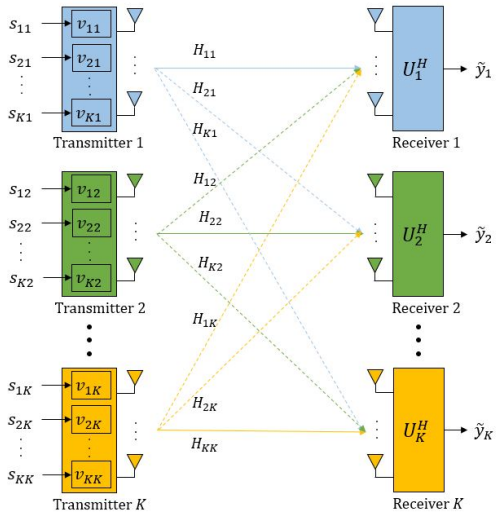

Fig. 2. K device MIMO Network

The information symbol s_{ij} from the j^{th} transmitter to the i^{th} receiver is precoded using the vector v_{ij} as shown below.

$$x_j = \sum_{i=1}^{K} v_{ij} s_{ij} \tag{2}$$

Where x_j is the transmit signal vector from the j^{th} transmitter.

If P_j is the total power available at the j^{th} transmitter, the transmit signal vector is subject to the following constraint,

$$Tr(x_j^H x_j) \leq P_j \tag{3}$$

TABLE II
PARAMETERS

Parameter	Description	Size
K	Number of ENodeBs and number of IoT devices	
M	Number of antennas per ENodeB and IoT device	
H_{ij}	Channel matrix from the j^{th} transmitter to the i^{th} receiver	$M \times M$
x_j	Transmit signal vector from j^{th} transmitter	$M \times 1$
s_{ij}	Symbol to be transmitted from j^{th} transmitter to the i^{th} receiver	
v_{ij}	Precoder for the symbol from j^{th} transmitter to the i^{th} receiver	$M \times 1$
P_j	Total power available at the j^{th} transmitter	
y_i	Signal received by the i^{th} receiver	$M \times 1$
n_i	Noise experienced by the i^{th} receiver	$M \times 1$
σ^2	Noise variance	
U_i	Zero forcing decoding matrix at the i^{th} receiver	$M \times M$
$H_{int}^{(i)}$	Set of aligned interfering column vectors at the i^{th} receiver	$M \times \frac{K(K-1)}{2}$
R_i	Residual interference at the i^{th} receiver	

The signal received at the i^{th} receiver y_i, is shown by,

$$\begin{aligned} y_i &= \sum_{j=1}^{K} H_{ij}x_j + ni \\ &= \underbrace{\sum_{j=1}^{K} H_{ij}v_{ij}s_{ij}}_{\text{Desired signal}} + \underbrace{\sum_{j=1}^{K}\sum_{k=1,\neq i}^{K} H_{ij}v_{kj}s_{kj}}_{\text{interference}} + n_i \end{aligned} \tag{4}$$

The first term in equation (4) is the desired signal vector intended for the i^{th} receiver, transmitted by the K transmitters. The second term represents the $K(K-1)$ interfering signal vectors. H_{ij} is the full rank channel matrix from the j^{th} transmitter to the i^{th} receiver. The noise level is denoted by n_i. We assume that the noise is Gaussian with zero mean and variance σ^2.

B. Zero forcing Beamformer

The beamformer is responsible for nulling out the interference signals such that each receiver is left only with its desired signal. As in [14], we use a zero forcing beamformer, U_i at each receiver i. The column vectors of U_i are orthogonal to the vector space spanned by the interfering signals. This means that by applying the beamformer to the received signal y_i, the second term in equation (4) is forced to zero.

The output signal vector after applying the beamformer is as shown below,

$$\begin{aligned} \tilde{y_i} &= U_i^H \cdot y_i \\ &= U_i^H \sum_{j=1}^{K} H_{ij}v_{ij}s_{ij} + \underbrace{U_i^H \cdot \sum_{j=1}^{K}\sum_{k=1,\neq i}^{K} H_{ij}v_{kj}s_{kj}}_{=0} + U_i^H n_i \end{aligned} \tag{5}$$

In order to achieve perfect interference cancellation, certain prerequisite conditions need to be met [14]. These are described below.

Prerequisite 1: At each receiver, interfering signals coming from the same transmitter, cannot be aligned in the same direction. For the j^{th} transmitter and i^{th} receiver this can be represented as follows,

$$H_{ij}v_{kj} \neq H_{ij}v_{lj} \quad i \neq k \neq l \tag{6}$$

Prerequisite 2: For a given K device system, there will be $K(K-1)$ interfering signals. $K-1$ interfering signals should be aligned in each of the K dimensions. This is written as,

$$span(H_{im}v_{km}) = span(H_{in}v_{ln}) \quad k,l \neq i \tag{7}$$

In the next subsection we present an example showing how to apply the prerequisites in determining the precoders and beamformers.

C. Example

We assume that there are 3 transmitters and receivers ($K = 3$) each having 6 antennas ($M = 6$). Each receiver will receive 3 desired signal vectors and 6 interference vectors. We reproduce the equations from [14] to obtain all the precoder vectors. First, a matrix E is defined,

$$\begin{aligned} E = &(H_{31})^{-1}H_{33}(H_{13})^{-1}H_{12}(H_{22})^{-1}H_{23}(H_{13})^{-1}H_{11} \\ &\times (H_{21})^{-1}H_{23}(H_{33})^{-1}H_{32}(H_{12})^{-1}H_{11}(H_{31})^{-1}H_{32} \\ &\times (H_{22})^{-1}H_{21} \end{aligned} \tag{8}$$

We can then start determining the $K^2(=9)$ precoder vectors. The first step is to assume a value for v_{11}. We do this by arbitrarily selecting any one of two eigen vectors of E. With v_{11}, we can find the rest of the precoders from equation (9) below.

$$\begin{aligned} v_{12} &= (H_{22})^{-1}H_{21}v_{11} \quad v_{31} = (H_{21})^{-1}H_{23}v_{13} \\ v_{21} &= (H_{31})^{-1}H_{32}v_{12} \quad v_{33} = (H_{13})^{-1}H_{11}v_{31} \\ v_{22} &= (H_{12})^{-1}H_{11}v_{21} \quad v_{32} = (H_{22})^{-1}H_{23}v_{33} \\ v_{13} &= (H_{33})^{-1}H_{32}v_{22} \quad v_{23} = (H_{13})^{-1}H_{12}v_{32} \end{aligned} \tag{9}$$

The equations listed in (9) are derived from the equations in column 2 of Table III. The equations in column 2 have been derived by applying the prerequisites shown above. It must be noted that there will be $\frac{K(K-1)}{2}$ span equations. We have found that there can be more than one way of selecting equations from the two prerequisites. A second set of span equations that also gives perfect interference cancellation are shown in column 3 of Table III. The zero forcing beamformer matrix U_i is obtained by taking the singular value decomposition of the interference-aligned signal space as follows,

$$\begin{aligned} H_{int}^{(1)} &= \begin{bmatrix} H_{11}v_{21} & H_{11}v_{31} & H_{12}v_{32} \end{bmatrix} \\ &= \begin{bmatrix} \bar{U}_1^{(1)} & \bar{U}_1^{(0)} \end{bmatrix} \begin{bmatrix} \bar{\Lambda}_1 & 0 \\ 0 & 0 \end{bmatrix} \begin{bmatrix} \bar{V}_1^{(1)} & \bar{V}_1^{(0)} \end{bmatrix}^H \end{aligned} \tag{10}$$

Where $H_{int}^{(1)}$ is the set of aligned interfering column vectors at the first receiver. From (10) we can set $\bar{U}_1^{(0)} = U_1$, thus obtaining the zero forcing beamformer at the first receiver.

TABLE III
INTERFERENCE ALIGNMENT CONDITIONS, 3-DEVICE NETWORK

	IA conditions [14]	IA conditions - another example
Rx 1	span($H_{11}v_{21}$) = span($H_{12}v_{22}$)	span($H_{11}v_{21}$) = span($H_{12}v_{22}$)
	span($H_{11}v_{31}$) = span($H_{13}v_{33}$)	span($H_{11}v_{21}$) = span($H_{13}v_{33}$)
	span($H_{12}v_{32}$) = span($H_{13}v_{23}$)	span($H_{12}v_{32}$) = span($H_{13}v_{23}$)
Rx 2	span($H_{21}v_{11}$) = span($H_{22}v_{12}$)	span($H_{22}v_{12}$) = span($H_{21}v_{11}$)
	span($H_{21}v_{31}$) = span($H_{23}v_{13}$)	span($H_{22}v_{32}$) = span($H_{23}v_{33}$)
	span($H_{22}v_{32}$) = span($H_{23}v_{33}$)	span($H_{21}v_{31}$) = span($H_{23}v_{13}$)
Rx 3	span($H_{31}v_{11}$) = span($H_{33}v_{23}$)	span($H_{32}v_{22}$) = span($H_{31}v_{11}$)
	span($H_{31}v_{21}$) = span($H_{32}v_{12}$)	span($H_{32}v_{12}$) = span($H_{33}v_{13}$)
	span($H_{32}v_{22}$) = span($H_{33}v_{13}$)	span($H_{33}v_{23}$) = span($H_{31}v_{21}$)

Similarly we determine the beamformers at the second and third receivers by the following equations.

$$\begin{aligned} H_{int}^{(2)} &= \begin{bmatrix} H_{21}v_{11} & H_{21}v_{31} & H_{22}v_{32} \end{bmatrix} \\ &= \begin{bmatrix} \bar{U}_2^{(1)} & \bar{U}_2^{(0)} \end{bmatrix} \begin{bmatrix} \bar{\Lambda}_2 & 0 \\ 0 & 0 \end{bmatrix} \begin{bmatrix} \bar{V}_2^{(1)} & \bar{V}_2^{(0)} \end{bmatrix}^H \end{aligned} \tag{11}$$

and

$$\begin{aligned} H_{int}^{(3)} &= \begin{bmatrix} H_{31}v_{11} & H_{31}v_{21} & H_{32}v_{22} \end{bmatrix} \\ &= \begin{bmatrix} \bar{U}_3^{(1)} & \bar{U}_3^{(0)} \end{bmatrix} \begin{bmatrix} \bar{\Lambda}_3 & 0 \\ 0 & 0 \end{bmatrix} \begin{bmatrix} \bar{V}_3^{(1)} & \bar{V}_3^{(0)} \end{bmatrix}^H \end{aligned} \tag{12}$$

Where $H_{int}^{(2)}$ and $H_{int}^{(3)}$ are the sets of aligned interfering column vectors at the second and third receiver respectively.

D. Extension to higher order systems

We have taken the analysis in [14] one step further by applying the interference alignment scheme to a 4-device system. One possible set of interference alignment conditions is shown in Table IV.

TABLE IV
INTERFERENCE ALIGNMENT CONDITIONS, 4-USER NETWORK

	IA conditions	
Rx 1	span($H_{11}v_{21}$) = span($H_{12}v_{22}$)	span($H_{11}v_{31}$) = span($H_{14}v_{44}$)
	span($H_{13}v_{23}$) = span($H_{12}v_{42}$)	span($H_{12}v_{32}$) = span($H_{11}v_{41}$)
	span($H_{14}v_{24}$) = span($H_{13}v_{33}$)	span($H_{14}v_{34}$) = span($H_{13}v_{43}$)
Rx 2	span($H_{21}v_{11}$) = span($H_{24}v_{34}$)	span($H_{24}v_{14}$) = span($H_{21}v_{31}$)
	span($H_{22}v_{12}$) = span($H_{23}v_{33}$)	span($H_{21}v_{41}$) = span($H_{22}v_{42}$)
	span($H_{23}v_{13}$) = span($H_{22}v_{32}$)	span($H_{23}v_{43}$) = span($H_{24}v_{44}$)
Rx 3	span($H_{31}v_{11}$) = span($H_{32}v_{22}$)	span($H_{34}v_{14}$) = span($H_{33}v_{23}$)
	span($H_{32}v_{12}$) = span($H_{31}v_{21}$)	span($H_{31}v_{41}$) = span($H_{33}v_{43}$)
	span($H_{33}v_{13}$) = span($H_{34}v_{24}$)	span($H_{32}v_{42}$) = span($H_{34}v_{44}$)
Rx 4	span($H_{41}v_{11}$) = span($H_{43}v_{13}$)	span($H_{41}v_{21}$) = span($H_{44}v_{24}$)
	span($H_{42}v_{12}$) = span($H_{44}v_{34}$)	span($H_{42}v_{22}$) = span($H_{43}v_{23}$)
	span($H_{44}v_{14}$) = span($H_{42}v_{32}$)	span($H_{41}v_{31}$) = span($H_{43}v_{33}$)

To determine the $K^2(=16)$ precoders, it is required to find a set of 16 equations covering all the precoders from amongst the span equations shown in Table IV. A possible set of such equations is shown below.

$$\begin{aligned} v_{34} &= (H_{24})^{-1}H_{21}v_{11} \quad & v_{23} &= (H_{13})^{-1}H_{12}v_{42} \\ v_{43} &= (H_{13})^{-1}H_{14}v_{34} \quad & v_{22} &= (H_{42})^{-1}H_{43}v_{23} \\ v_{41} &= (H_{31})^{-1}H_{33}v_{43} \quad & v_{21} &= (H_{11})^{-1}H_{12}v_{22} \\ v_{32} &= (H_{12})^{-1}H_{11}v_{41} \quad & v_{12} &= (H_{32})^{-1}H_{31}v_{21} \\ v_{14} &= (H_{44})^{-1}H_{42}v_{32} \quad & v_{33} &= (H_{23})^{-1}H_{22}v_{12} \\ v_{31} &= (H_{21})^{-1}H_{24}v_{14} \quad & v_{24} &= (H_{14})^{-1}H_{13}v_{33} \\ v_{44} &= (H_{14})^{-1}H_{11}v_{31} \quad & v_{13} &= (H_{33})^{-1}H_{34}v_{24} \\ v_{42} &= (H_{32})^{-1}H_{34}v_{44} \quad & v_{11} &= (H_{41})^{-1}H_{43}v_{13} \end{aligned} \tag{13}$$

As in the case when $K = 3$, an E matrix is defined from the equations in (13) above. For the beamformers, as before, $H_{int}^{(1)}$ can be defined as,

$$\begin{aligned} H_{int}^{(1)} &= \begin{bmatrix} H_{11}v_{21} & H_{13}v_{23} & H_{14}v_{24} & H_{11}v_{31} & H_{12}v_{32} & H_{14}v_{34} \end{bmatrix} \\ &= \begin{bmatrix} \bar{U}_1^{(1)} & \bar{U}_1^{(0)} \end{bmatrix} \begin{bmatrix} \bar{\Lambda}_1 & 0 \\ 0 & 0 \end{bmatrix} \begin{bmatrix} \bar{V}_1^{(1)} & \bar{V}_1^{(0)} \end{bmatrix}^H \end{aligned} \tag{14}$$

and U_1 can be set to $\bar{U}_1^{(0)}$. Similar matrices can be written for the other receivers.

E. Non ideal case

It is to be noted that perfect interference cancellation through the use of the zero forcing beamformer is possible only if perfect Channel State Information (CSI) is available. We recognize that this is usually not the case and proceed to develop a closed form expression for the residual interference that gets through to the receivers. We characterize the residual interference by the Interference Margin which is defined as the deterioration of SNR as a result of co-channel interference [15]. The following equations cited and summarized from [15] show the derivation of Interference Margin. We start by rewriting equation (5) as follows,

$$\tilde{y_i} = U_i^H \sum_{j=1}^{K} H_{ij}v_{ij}s_{ij} + \underbrace{U_i^H \cdot \sum_{j=1}^{K} \sum_{k=1,\neq i}^{K} H_{ij}v_{kj}s_{kj}}_{=0} + U_i^H n_i + \sum_{j=1}^{K} \sum_{k=1,\neq i}^{K} R_{kj} \tag{15}$$

Where the last term in equation (15) represents the total residual interference at the i^{th} receiver after applying the zero forcing beamformer. This is shown in equation (16) below.

$$R_i = \sum_{j=1}^{K} \sum_{k=1,\neq i}^{K} R_{kj} \tag{16}$$

Let Y_i be the total residual interference power at the i^{th} receiver such that,

$$Y_i = \sum_{j=1}^{K} \sum_{k=1,\neq i}^{K} |R_{kj}|^2 \tag{17}$$

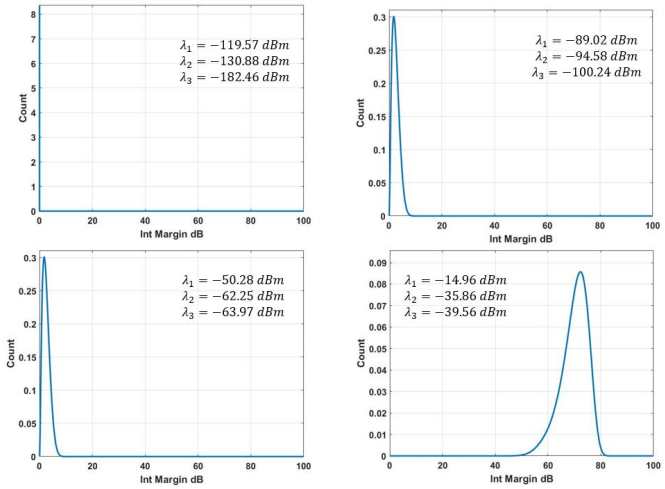

Fig. 3. Interference margin plots for various residual interference powers resulting from channel estimation errors.

We model the residual interference as a random variable that follows a Rayleigh distribution. Therefore Y_i would follow an exponential distribution with mean $\lambda_j = E[\sum_{k=1,\neq i}^{K} |R_{kj}|^2]$. It follows that Y_i is the sum of K independent random variables and its Moment Generating Function (MGF) is given by,

$$MGF_{Y_i}(t) = \prod_{j=1}^{K} \frac{1}{1 - t\lambda_j} \tag{18}$$

Assuming that all λ_j are distinct, taking the inverse of the MGF to obtain the probability density function,

$$f_{Y_i}(y) = \sum_{j=1}^{K} \frac{c_j}{\lambda_j} e^{-\frac{y}{\lambda_j}} \tag{19}$$

Where c_j represents the coefficients of partial fraction decomposition of the product in (18). Now we need to obtain the equation for the distribution of interference margin, Φ.

Given the PDF of Y_i, we need to find the PDF of

$$\Phi_i = \frac{Y_i + \sigma^2}{\sigma^2} \tag{20}$$

given by $f_{\Phi_i}(\phi)$.

By applying the random variable transformation rule we obtain the PDF of interference margin as,

$$\begin{aligned} f_{\Phi_i}(\phi) &= \sigma^2 f_{Y_i}(\sigma^2(\phi - 1)) \\ &= \sigma^2 \sum_{j=1}^{K} \frac{c_j}{\lambda_j} e^{-\frac{\sigma^2(\phi-1)}{\lambda_j}} \end{aligned} \tag{21}$$

Fig. 3 shows interference margin plots for various levels of residual interference. An additional random variable transformation has been applied to (21) to convert it into dB before plotting. It can be seen from the plots that as the channel estimation errors increase, the residual interference reaching the receivers also increases.

III. Self Organizing Networks (SON) for IoT Interference Alignment

In this section we introduce a protocol for self-organizing interference alignment in dense IoT networks.

A. Motivation for the use of SON

A Self Organizing Network is one in which intelligence and autonomous adaptive capabilities are added to the network. More specifically, SONs are intelligent systems that are capable of learning from their environment and can adapt to statistical variations in input stimuli [16]. SON frameworks can also be modeled as adaptive functional networks that can detect changes and make intelligent decisions to maximize or minimize the effects caused by these changes [17]. In [18] SON mechanisms are represented as feedback control loops that monitor pre-defined network performance indicators usually to optimize certain parameters.

SON concepts have been widely applied in solutions to the problem of interference in wireless networks. The most direct approach for interference control as pointed out by [19] would be to turn off network nodes when they are inactive. In [20], the authors point out that a single fixed reuse model is not sufficient to cope with the varying traffic patterns. They have proposed an interference mitigation scheme in which the network can change to a more optimum frequency reuse pattern. Another approach, as adopted by [21] maximizes spectral efficiency in relay-enhanced networks by self- organization of antenna tilts. Additionally, a comprehensive survey detailing the advances of SON in the past decade is provided in [22].

With regards to 5G IoT networks, SON finds a direct use case in dense networks where it becomes virtually impossible to configure and monitor networks manually. In particular, dense IoT networks exhibit highly varying traffic and co-channel interference patterns as more and more devices connect to the network. Each time a new device connects to the network, the precoders and beamformers across all nodes have to be re-designed in order to maintain the interference alignment in the network. We envision a network that can apply SON techniques to facilitate this re-design.

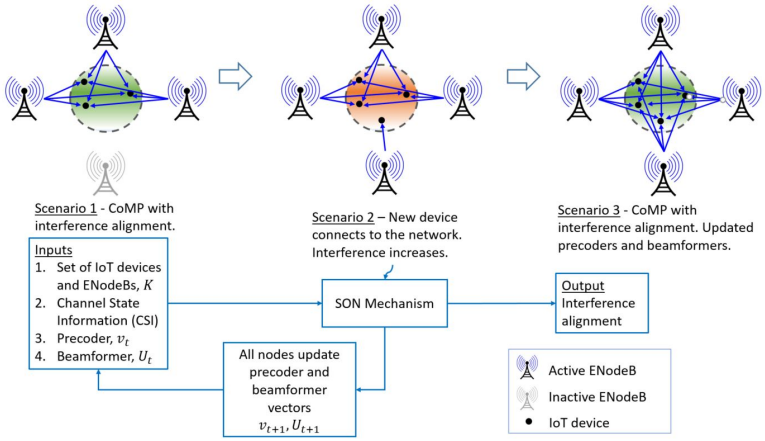

Fig. 4. SON protocol for interference alignment

Algorithm 1: SON protocol for IoT Interference Alignment

Input : IoTDevices and ENodeBs, $\{1 \dots K\}$
Input : Interference Margin Threshold, Φ_{th}
Input : Channel Matrix, H
$t = 0$;
while $t \geq 0$ **do**
  for k *in IoTDevices* **do**
    Calculate precoders, $v_t(k)$;
    Calculate beamformers, $U_t(k)$;
    Calculate residual interference margin, $\Phi(k)$;
    if $\Phi(k) > \Phi_{th}$ **then**
      Scan for new connected devices;
    end
  end
  IoTDevices = $\{1 \dots K, K+1\}$;
  ENodeBs = $\{1 \dots K, K+1\}$;
  $t = t + 1$;
end

B. SON protocol for interference alignment

The proposed SON protocol is shown in Fig. 4. The inputs to the system would be network parameters such as ENodeB and IoT device positions, Channel State Information (CSI), the precoder and beamformer. We model the SON framework as having a feedback loop that allows the inputs to be changed in response to the output which in this case is interference. In scenario 1, when there are 3 devices and 3 ENodeBs, all the nodes implement the interference alignment equations described above, to cancel the interference. Scenario 2 shows the case in which a new device is turned on. This device first connects to its nearest ENodeB which in this case is a fourth ENodeB that was previously inactive. The prior interference alignment becomes disturbed as a result of the new device. This triggers the SON mechanism which then reorganizes the network by first reconfiguring the CoMP such that all 4 devices are served by all 4 ENodeBs. Secondly, it facilitates an update of the precoders and beamformers in all the nodes to achieve interference alignment once again (scenario 3). This protocol is also delineated in Algorithm 1.

IV. Conclusion

In this paper we have investigated a perfect interference alignment scheme for MIMO systems. We have proposed the application of this scheme to a 5G IoT architecture. We have also defined a fast method for obtaining the residual interference profile in cases of imperfect channel estimation.

A. Acknowledgment

We gratefully acknowledge the support of the DoD, Testing Evaluation and Control of Heterogeneous Large Systems of Autonomous Vehicles (TECHLAV) research grant and the Office of Naval Research (ONR) N00014-16-R-BA01 grant for naval communications.

References

[1] Ericsson, "5g radio access - research and vision, white paper," *Online*, pp. http://www.ericsson.com/res/docs/whitepapers/wp–5g.pdf, 2013.
[2] J. Zander and P. Mhnen, "Riding the data tsunami in the cloud: Myths and challenges in futurewireless access," *IEEE Communications Magazine*, vol. 51, no. 3, pp. 145–151, March 2013.
[3] R. Heath, T. Wu, Y. Kwon, and A. Soong, "Multiuser mimo in distributed antenna systems," *2010 Conference Record of the Forty Fourth Asilomar Conference on Signals, Systems and Computers*, pp. 1202–1206, 2010.
[4] S. Lee, S. Moon, H. Kong, and I. Lee, "Optimal beamforming schemes and its capacity behavior for downlink distributed antenna-systems," *IEEE Transactions on Wireless Communications*, vol. 12, no. 6, pp. 2578–2587, March 2013.
[5] R. Heath, "What is the role of mimo in future cellular networks: Massive coordinated mmwave," *IEEE CTS COMSOC-SP and IM Joint DLT Meeting*, 2013.
[6] N. Bhushan, "Network densifiction: the dominant theme for wireless evolution into 5g," *IEEE Communication Magazine*, vol. 52, no. 2, pp. 82–89, Feb., 2014.
[7] C. Mobile, "C-ran: The road towards green ran," *White Paper*, 2011.
[8] D. Sabella, P. Rost, Y. Sheng, E. Pateromichelakis, U. Salim, P. Guitton-Ouhamou, M. Girolamo, and G. Giuliani, "Ran as a service: Challenges of designing a flexible ran architecture in a cloud-based heterogeneous mobile network," *Future Network and Mobile Summit*, pp. 1–8, July 2013.
[9] M. HadZialic, B. Dosenovic, M. Dzaferagic, and J. Musovic, "Cloudran: Innovative radio access network architecture," *2013 55th International Symposium in ELMAR*, pp. 115–120, 2013.
[10] 3GPP.org, *Narrowband Internet of Things (NB-IoT); Technical Report for BS and UE radio transmission and reception*. 3GPP TR 36.802, 2016.
[11] A. Bahga and V. Madisetti, *Internet of Things A Hands-On Approach*. Bahga and Madisett, 2014.
[12] V. R. Cadambe and S. A. Jafar, "Interference alignment and degrees of freedom of the k-user interference channel," *IEEE Transactions on Information Theory*, vol. 54, no. 8, pp. 3425–3441, 2008.
[13] K. Gomadam, V. R. Cadambe, and S. A. Jafar, "Approaching the capacity of wireless networks through distributed interference alignment," in *Global Telecommunications Conference, 2008. IEEE GLOBECOM 2008. IEEE*, pp. 1–6, IEEE, 2008.
[14] S.-H. Park and Y.-C. Ko, "K-user mimo x network system with perfect interference alignment," in *Communications (ICC), 2011 IEEE International Conference on*, pp. 1–5, IEEE, 2011.
[15] M. Jaber, N. Akl, Z. Dawy, and E. Yaacoub, "Statistical link budget analysis approach for lte cellular network dimensioning," in *European Wireless 2014; 20th European Wireless Conference; Proceedings of*, pp. 1–6, VDE, 2014.
[16] S. Haykin, "Cognitive radio: brain-empowered wireless communications," *IEEE journal on selected areas in communications*, vol. 23, no. 2, pp. 201–220, 2005.
[17] A. Spilling, A. Nix, M. Beach, and T. Harrold, "Self-organisation in future mobile communications," *Electronics & Communication Engineering Journal*, vol. 12, no. 3, pp. 133–147, 2000.
[18] A. Tall, R. Combes, Z. Altman, and E. Altman, "Distributed coordination of self-organizing mechanisms in communication networks," *IEEE Transactions on Control of Network Systems*, vol. 1, no. 4, pp. 328–337, 2014.
[19] I. Ashraf, L. T. Ho, and H. Claussen, "Improving energy efficiency of femtocell base stations via user activity detection," in *Wireless Communications and Networking Conference (WCNC), 2010 IEEE*, pp. 1–5, IEEE, 2010.
[20] A. Imran, M. A. Imran, and R. Tafazolli, "A novel self organizing framework for adaptive frequency reuse and deployment in future cellular networks," in *Personal Indoor and Mobile Radio Communications (PIMRC), 2010 IEEE 21st International Symposium on*, pp. 2354–2359, IEEE, 2010.
[21] A. Imran, M. A. Imran, A. Abu-Dayya, and R. Tafazolli, "Self organization of tilts in relay enhanced networks: A distributed solution," *IEEE Transactions on Wireless Communications*, vol. 13, no. 2, pp. 764–779, 2014.
[22] O. G. Aliu, A. Imran, M. A. Imran, and B. Evans, "A survey of self organisation in future cellular networks," *IEEE Communications Surveys & Tutorials*, vol. 15, no. 1, pp. 336–361, 2013.